Polymer 51 (2010) 2690–2699

Contents lists available at ScienceDirect

Polymer

journal homepage: www.elsevier.com/locate/polymer

Composites of polyamide 6 and silicate nanotubes of the mineral halloysite: Influence of molecular weight on thermal, mechanical and rheological properties

Ulrich A. Handge [a,*], Katrin Hedicke-Höchstötter [b], Volker Altstädt [a]

[a] Department of Polymer Engineering, Faculty of Engineering Science, University of Bayreuth, Universitätsstrasse 30, 95447 Bayreuth, Germany
[b] Polymer Engineering, Technical University of Hamburg-Harburg, Neuhöfer Strasse 23, 21107 Hamburg, Germany

ARTICLE INFO

Article history:
Received 18 January 2010
Received in revised form
16 April 2010
Accepted 19 April 2010
Available online 24 April 2010

Keywords:
Nanocomposites
Halloysite
Mechanical reinforcement

ABSTRACT

In this work, the potential of silicate nanotubes of the naturally occurring mineral halloysite as filler for polyamide 6 (PA 6) nanocomposites is evaluated. Several PA 6/halloysite composites with 0 wt% to 30 wt % filler loading using two different grades of PA 6 were prepared. In order to elucidate the influence of molecular weight on the properties of the nanocomposites, mechanical resp. rheological experiments (i) below the glass transition temperature T_g of PA 6, (ii) between T_g and the melting temperature T_m of PA 6 and (iii) above T_m were performed. Our investigations reveal that the addition of halloysite nanotubes favours the formation of the γ-modification for the low molar mass PA 6. Furthermore, the storage modulus, the tensile modulus and the yield stress of the composites increase with concentration of halloysite, an effect which is strongly pronounced at very low filler fractions for the low molar mass PA 6 composites. The increase of the storage modulus which was measured in dynamic-mechanical experiments is mostly dominant in the temperature interval from 55 °C to 100 °C, i.e. above the glass transition temperature of PA 6. Rheological investigations showed that the shear viscosity is only moderately increased by the addition of a low fraction of halloysite to PA 6, and nanocomposites with 30 wt% halloysite can be still processed. In summary, halloysite nanotubes are promising and inexpensive candidates for increasing the stiffness of PA 6 while maintaining very good flow properties.

1. Introduction

The reinforcement of polymers by the addition of nanofillers such as clay minerals or carbon nanotubes has attracted much attention in polymer engineering since many decades [1–14]. Silicate nanoplatelets, e.g., montmorillonite, are frequently used as fillers in polymer nanocomposites [11,12]. Besides the combination of the properties of polymer matrix and fillers and processing as conventional plastics, the small dimensions of the nanofillers lead to peculiar properties such as transparency and very good surface properties. Furthermore, heat resistance, flame retardance, wear and barrier properties of polymers can be enhanced by adding nanofillers [2].

In recent years, a variety of fillers has been investigated for reinforcement of thermoplastic polymers. The large intrinsic stiffness of montmorillonite leads to a nanocomposite with a large modulus and strength [15]. In this work, we focus on silicate nanotubes of the mineral halloysite which combine the chemistry of montmorillonite and the geometry of carbon nanotubes. The chemical formula of halloysite is $Al_2[Si_2O_5(OH)_4]\cdot 2H_2O$. It mainly consists of hollow tubes with dimensions of up to 10 μm in length and an outer diameter in the order of 30–100 nm [16]. These dimensions result in a high aspect ratio and a very high surface. The hollow core of halloysite nanotubes allows to deposit other molecules which can be continuously released. From a mineralogical point of view, halloysite is a mineral similar to kaolin which is frequently used as filler for polymers. Halloysite occurs as a weathering product of volcanic stones from rhyolitic to granitic compositions and is commercially used for tableware. Thus, halloysite nanotubes appear as an interesting, low-priced candidate for fabrication of high performance materials based on polymers, a possibly cost-effective alternative for specific applications in comparison to the expensive carbon nanotubes.

The mechanical properties of composites based on micron-sized mineral fillers such as kaolin, talc and fibrous wollastonite were studied in several works. In the study of Unal et al. different PA 6 composites filled with minerals were compared [17]. Composites of PA 6 and wollastonite showed the best mechanical performance because of the high aspect ratio of the filler. In contrast to these minerals, halloysite belongs to the class of nanofillers. A series of publications was devoted to the properties of polymer/halloysite

* Corresponding author. Tel.: +49 921 55 7476; fax: +49 921 55 7473.
E-mail address: ulrich.handge@uni-bayreuth.de (U.A. Handge).

0032-3861/$ – see front matter © 2010 Elsevier Ltd. All rights reserved.
doi:10.1016/j.polymer.2010.04.041

composites [18–24]. The mechanical properties of polypropylene/halloysite composites were investigated in Ref. [25]. The study of Guo et al. revealed that the addition of halloysite increases the fraction of the γ-phase in polyamide 6 and accelerates crystallization of polyamide 6 [26]. Ning et al. investigated the crystallization behaviour and the mechanical properties of polypropylene/halloysite composites [27]. In their work, only a very slight enhancement of the mechanical properties was observed which was explained by the constant crystallinity in the polypropylene matrix and the small length to diameter ratio of the halloysite nanotubes. Several authors focused on the effect of the addition of halloysite on the thermal stability and flame retardancy of polymers [28,29]. Halloysite nanotubes more than doubled the total burning time by developing a thermal insulation barrier at the surface of the composite. In recent works, modified halloysite was used for preparation of polymer/halloysite composites [30,31]. The influence of grafting of polypropylene (PP) to the surface of halloysite on the mechanical properties of PP/halloysite composites was studied in Ref. [30]. Guo et al. studied polyamide 6 nanocomposites based on modified halloysites. Both studies showed an increase of the mechanical properties for the composites with modified halloysite in comparison to the unmodified composites.

In a previous work, halloysite nanocomposites based on polyamide 6 were prepared, and dynamical mechanical analysis and tensile testing experiments at room temperature were carried out [32,33]. In addition to the increase of Young's modulus and tensile strength, the strain at break was increased by the addition of a low amount of halloysite nanotubes. This first analysis revealed that at room temperature the effect of adding halloysite nanofillers is mostly pronounced at low volume fractions of the filler. The objective of this work is to investigate the influence of molecular weight and temperature on the mechanical and rheological properties of the nanocomposites. Different series of PA 6/halloysite nanocomposites were prepared with a different molar mass of the PA 6 matrix. In each series, the concentration of halloysite varied from 0 wt% to 30 wt% and hence comprised a much larger composition range than the previous works. The temperature of the mechanical and rheological experiments was chosen such that experiments (i) below the glass transition temperature T_g of PA 6, (ii) in the interval between T_g and the melting temperature T_m of PA 6 and (iii) above T_m were performed. Thereby, the temperature dependence of the mechanical properties of PA 6/halloysite nanocomposites was elucidated.

2. Experimental

2.1. Materials

In this work, three series of polyamide 6 (PA 6) nanocomposites which were filled with silicate nanotubes of the mineral halloysite were prepared. First, the influence of a large fraction of halloysite nanotubes on the properties of polyamide 6 was investigated. The matrix material was PA 6 Ultramid® B27 and was supplied by BASF SE (Ludwigshafen, Germany). Tubular halloysites were provided by Imerys Tableware Ltd. (Auckland, New Zealand). The density of neat halloysite is approximately 2.59 g/cm^3. For the purpose of purification, the halloysite clay passes through a surge tank and a centrifuge. After passing through a series of mixing tanks it is fed to a filter press and finally dried. The halloysite was not grinded such that the aspect ratio of the halloysite tubes was not altered. The weight fraction of halloysite was 0, 10, 20 and 30 wt%. Polyamide 6 and halloysite powder were premixed and subsequently compounded using a twin screw extruder ZE 25 (Berstorff, Hannover, Germany) at 265 °C. The screw speed was 180 min^{-1}. These composites are denoted by B27/HA G composites.

In a second step, the influence of the molar mass of PA 6 on the properties of PA 6/halloysite nanocomposites was studied. Two different lots of PA 6 were chosen, i.e. PA 6 Ultramid® B27 E and PA 6 Ultramid® B40, respectively (BASF SE, Ludwigshafen, Germany). The molar mass of PA 6 B40 was larger than the molar mass of PA 6 B27 E, see Table 1. The weight fraction φ of the halloysite fillers in the second series was 0, 0.2, 0.5, 1.0, 2.0, 5.0, 10.0, 20.0 and 30.0 wt%. The pellets of PA 6 and the powder of halloysite were premixed and dried at 80 °C in vacuum before compounding. Then the compounds were prepared using a twin screw extruder ZE 25 (Berstorff, Hannover, Germany). The processing temperature was 230 °C for these B27/HA R composites and 250 °C for these B40/HA R composites. In both cases, the number of screw rotations was 220 min^{-1}. The neat PA 6 B27 E and B40 were extruded under the same conditions as the nanocomposites.

2.2. Morphological studies

In order to determine the microstructure of the halloysite powder, the as-received powder of neat halloysite was suspended in acetone. Afterwards a droplet of the suspension was sprayed on a grid for transmission electron microscopy (TEM) studies. The TEM investigations were performed using a TEM of type LEO EM 922 Omega (Carl Zeiss, Oberkochen, Germany). The acceleration voltage was 200 kV.

Samples for morphological investigations of the composites were prepared by fracturing compression-moulded cylindrical plates which were cooled using liquid nitrogen. The samples were coated with a platin layer of 1 nm thickness using a sputtering device (Cressington 208 HR in the automatic mode). Then the morphology was studied using a scanning electron microscope that was equipped with a field emission cathode (FE-SEM Leo 1530 FE, Carl Zeiss, Oberkochen). The acceleration voltage was varied and ranged between 2 and 5 kV.

2.3. Thermal properties

The thermal stability of neat halloysite powder and selected PA 6/halloysite composites was determined by performing a thermal gravimetric analysis (TGA). A TGA/SDTA 851e (Mettler Toledo, Gießen, Germany) was used for the investigations. The tests were performed in the temperature range from 25 °C to 1100 °C in a nitrogen atmosphere. The heating rate was 10 K/min and the weight of the sample was approximately 11 mg. The halloysite powder was used as-received without drying. The nanocomposites were dried at 80 °C in vacuum for 14 days.

In order to study the thermal properties of the materials using differential scanning calorimetry (DSC), samples of extruded polyamide 6 and of the composites were stored under vacuum at 80 °C for at least three days. A DSC 821e (Mettler-Toledo, Gießen, Germany) was used at a heating/cooling rate of 10 K/min in the temperature interval 0–270 °C for determination of the thermal transitions. In order to eliminate the thermal history of the materials, a heating–cooling–heating cycle was applied. Then the thermal transitions were analyzed based on the cooling and the

Table 1
Physical properties of PA 6 Ultramid® B27 E and PA 6 Ultramid® B40 (BASF SE, Ludwigshafen, Germany).

	T_g (°C)	T_m (°C)	M_n (g/mol)	M_w (g/mol)	M_w/M_n	η_0 at 240 °C (Pa s)
PA 6 B27 E	54	221	21 800	65 200	3.0	400
PA 6 B40	53	220	28 400	116 000	4.1	3500

second heating cycle. The predried pellets of the extruded compounds had a net weight in the order of 5–10 mg.

Furthermore, dynamic-mechanical analysis (DMA) measurements were performed using an RDA III (Rheometric Scientific, Piscataway, USA) in the torsion mode. Samples with rectangular cross sections were cut from injection-moulded tensile bars (cf. Section "Mechanical properties") with dimensions of $2.0 \times 4.0 \times 30.0$ mm^3. Before the experiments, the samples were dried at 80 °C for seven days under vacuum. The frequency f was set to $f = 1$ Hz. The amplitude of shear strain was 0.15% and the heating rate was 3 K/min. Measurements were performed in the temperature interval −120–215 °C and also in the interval 25–215 °C.

2.4. Wide angle X-ray diffraction measurements

The crystalline structure of PA 6 and the composites were determined using wide angle X-ray diffraction (WAXD) measurements. These experiments were carried out in the reflection mode with extruded pellets. An X-ray diffractometer XRD 3000 P (Seifert, Ahrensburg, Germany) which was equipped with a Cu Kα radiation source ($\lambda = 1.5418$ Å, operated at 40 kV and 30 mA) was used for the investigations in the interval $2\theta = 5°–50°$. A step of 0.03° was taken in all scans.

2.5. Mechanical properties

In order to investigate the mechanical properties of the halloysite composites standard dumbbell specimens (S2 bars according to DIN EN ISO 527-2) with a thickness of 2 mm and a width of 4 mm were prepared by injection moulding. Prior to injection moulding the extruded pellets were dried in a convection dryer at 80 °C. The injection moulding device was an Allrounder 420C 800-250 Jubilee (Arburg, Loßburg, Germany). The cylinder temperature of injection moulding was 270 °C and the screw rotation speed was 200 min^{-1}. The injection-moulded specimens were dried at 80 °C for 7 days in vacuum. The drying interval of 7 days was chosen such that it was long enough to guarantee almost moisture-free samples and to minimize the effect of further crystallization of the PA 6 matrix. Then tensile tests under uniaxial loading were performed using a universal testing machine (Zwick 1455 with a 10 kN load cell). The tests were carried out at room temperature and at 80 °C (heating time 10 min) following the ISO standard 527 with a cross-head velocity of 5 mm/min. Measurements with at least 7 samples of each material were performed, and the nominal stress–strain diagram was analyzed. In all experiments, Young's modulus was measured with a cross-head velocity of 1 mm/min and analyzed in the interval of linear stress–strain behaviour. The yield stress corresponds to the first maximum of the nominal stress–strain diagram.

2.6. Rheological properties

Pellets of extruded neat polyamide 6 and the nanocomposites were dried in vacuo at 80 °C for at least three days and subsequently compression-moulded into cylindrical samples at 240 °C for 5 min. Before the rheological experiments, the samples were stored again in vacuo. The flow properties at low shear rates and small deformations were probed by linear viscoelastic shear oscillations. The measurement temperature was 240 °C. The shear amplitude γ_0 was $\gamma_0 = 0.10$ such that the measurements were performed in the linear viscoelastic regime. The diameter of the cylindrical samples was 24 mm and their thickness was 2 mm. The melting time of the sample was set to 5 min. The measurements were performed in a nitrogen atmosphere in order to avoid degradation of PA 6.

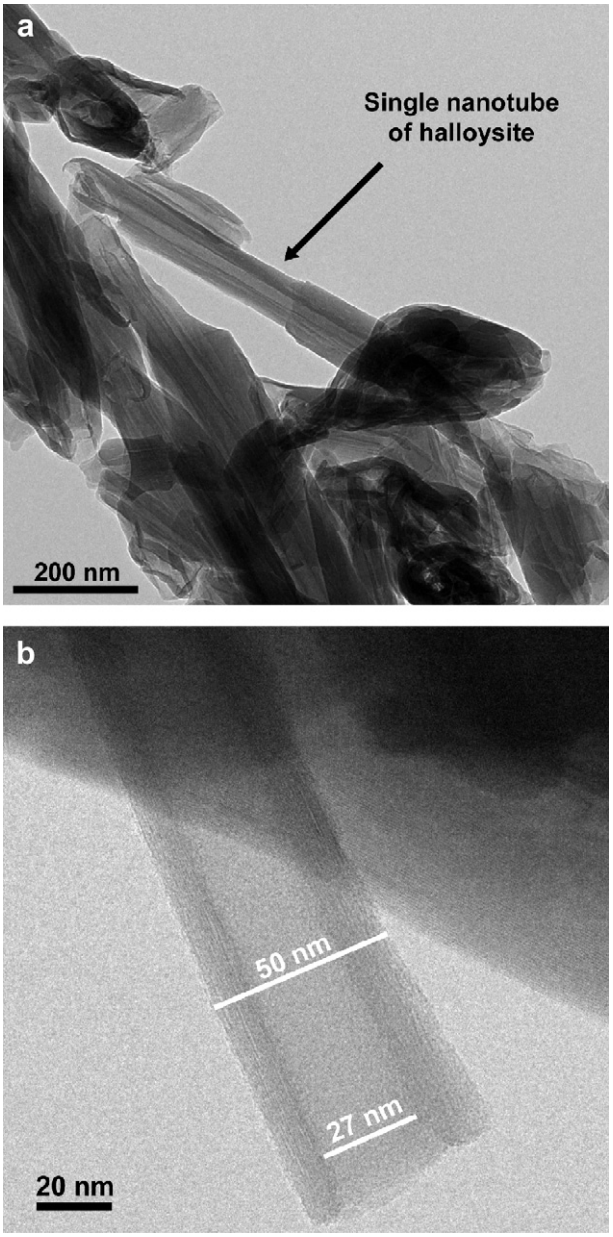

Fig. 1. Transmission electron micrographs of nanotubes of the mineral halloysite. (a) A typical cluster of the nanotubes as-received. (b) High resolution micrograph of a single silicate nanotube.

Measurements of the stationary viscosity at large shear rates were performed using a capillary rheometer Rheograph 6000 (Göttfert, Buchen, Germany). The diameter of the piston was 12 mm. Three dies with a diameter of 1 mm and a length of 10, 20 and 30 mm, respectively, were used. The test temperature was 240 °C and the melting time in the barrel was 5 min. The Bagley and the Rabinowitch–Weissenberg corrections were applied in order to determine the true viscosity from the apparent quantities.

Rheotens measurements at 240 °C were performed in order to determine the properties in melt elongation. A Rheotens tester 71.97 combined with a Rheograph 6000 (Göttfert, Buchen, Germany) was used. The diameter of the piston of the Rheograph 6000 was 12 mm and the piston velocity was 0.3 mm s^{-1}. The length of the circular die (diameter $d = 2$ mm) was $l = 30$ mm. The apparent shear rate in the die was 43.2 s^{-1}. The spin length L_s was

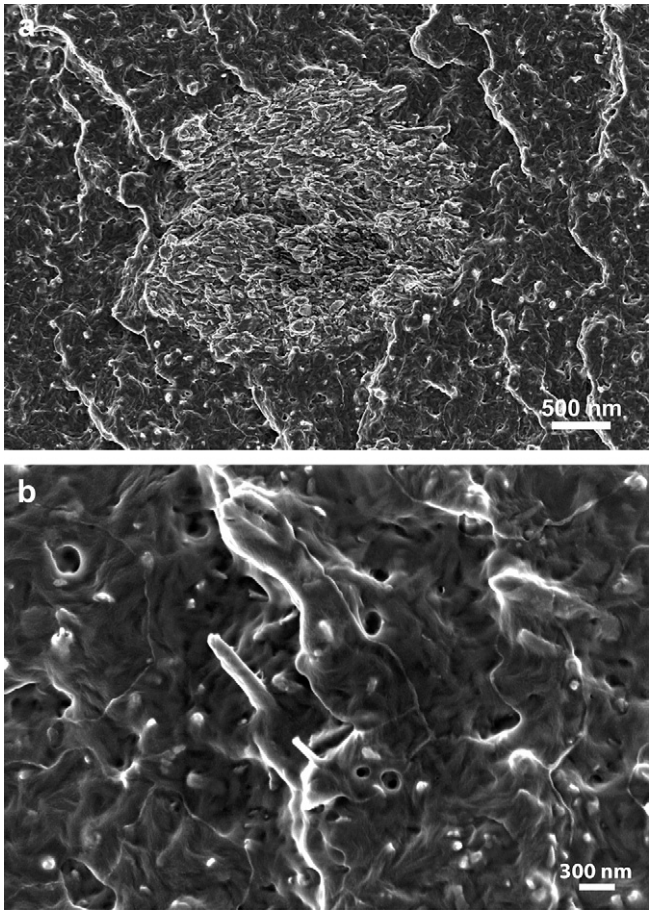

Fig. 2. Scanning electron micrographs of the B27/HA R composite with a concentration of 20 wt% of silicate nanotubes using different magnifications ((a) and (b)).

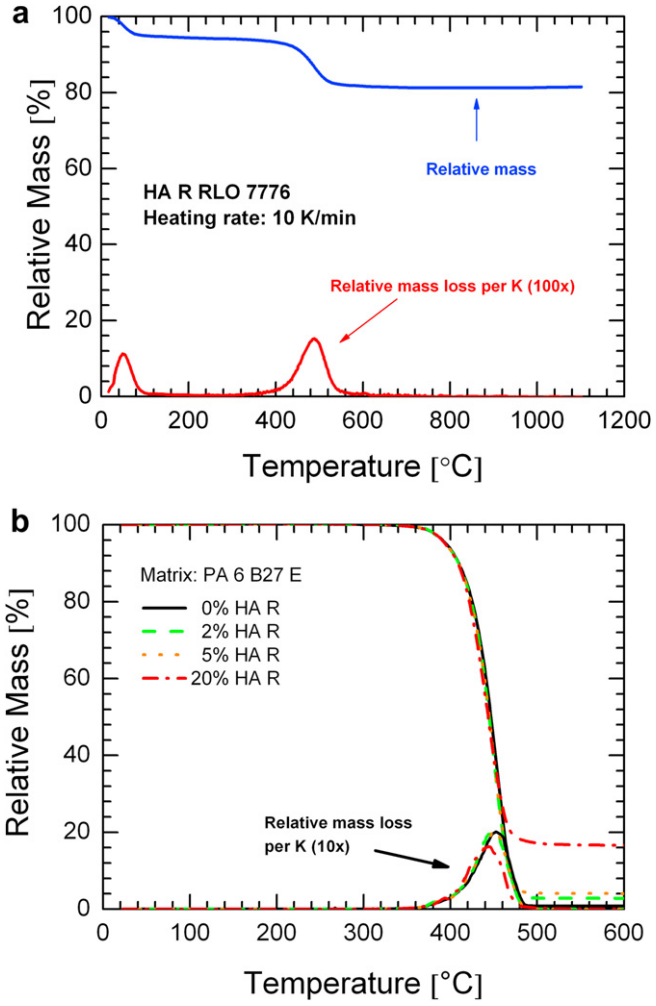

Fig. 3. Relative mass m and relative mass loss $-dm/dT$ (multiplied by a factor of (a) 100 and (b) 10) of (a) the halloysite powder as received and (b) selected B27/HA R composites measured by thermal gravimetric analysis (TGA). The heating rate was 10 K/min. A nitrogen atmosphere was applied.

equal to 95.0 mm, and the extrusion velocity of the strand $v_0 = 10.8$ mm s^{-1}. The acceleration of the wheels was set to 12 mm s^{-2}.

3. Results

3.1. Morphology

Fig. 1 shows transmission electron micrographs of the as-received powder of the mineral halloysite. The halloysite powder consists of agglomerates of hollow nanotubes, see Fig. 1(a). Even after suspending the powder in acetone agglomerates of halloysite nanotubes are visible. A part of a single cylindrical silicate nanotube is presented in Fig. 1(b). The nanotubes are tubular and have a hollow core. The outer diameter ranges between 30 and 100 nm and the diameter of the inner core roughly is 20–30 nm. The micrographs reveal that some halloysite fillers have sharp edges which are possible sources of defects leading to stress concentration. Generally, the size distribution of halloysite is quite large, since it is a natural product.

After compounding, the PA 6 nanocomposites attained a more brown color with increasing halloysite concentration. The scanning electron micrographs of the PA 6 B27/halloysite nanocomposites reveal that the halloysite nanotubes are in general uniformly dispersed, see Fig. 2(a). Furthermore the micrographs indicate that the single nanotubes are wetted by PA 6 (Fig. 2(b)) which leads to a good interaction between the surface of the nanotubes and the matrix. However, some agglomerates are also visible. Based on the SEM micrographs, the estimated fraction of agglomerates was in the order of 20% of the total amount of halloysite. The analysis of the SEM micrographs reveals that agglomeration of halloysite was more pronounced at larger filler fractions.

3.2. Thermal properties

The results of the thermal gravimetric analysis are shown in Fig. 3. A weight loss of approx. 5 wt% is observed up to 100 °C for the halloysite powder which can be attributed to the loss of water, see Fig. 3(a). A second large step is located with a peak at approximately 488 °C. This loss of mass is caused by the decomposition of the hydroxyl groups. The data show that halloysite is thermally stable up to 400 °C which is clearly above the processing temperature of polyamide 6. Consequently, halloysite nanotubes may also be adequate fillers for high temperature thermoplastic polymers. The TGA curves of the composites are only marginally shifted towards lower temperatures when compared to neat PA 6, see Fig. 3(b). Hence no significant influence of halloysite on the thermal properties of PA 6 was observed in the TGA experiments.

Fig. 4 presents the melting behaviour of neat PA 6, the B27/HA R and the B40/HA R composites. The melting peaks of the α- and the γ-modifications are also indicated [34,35]. The data of PA 6 B27

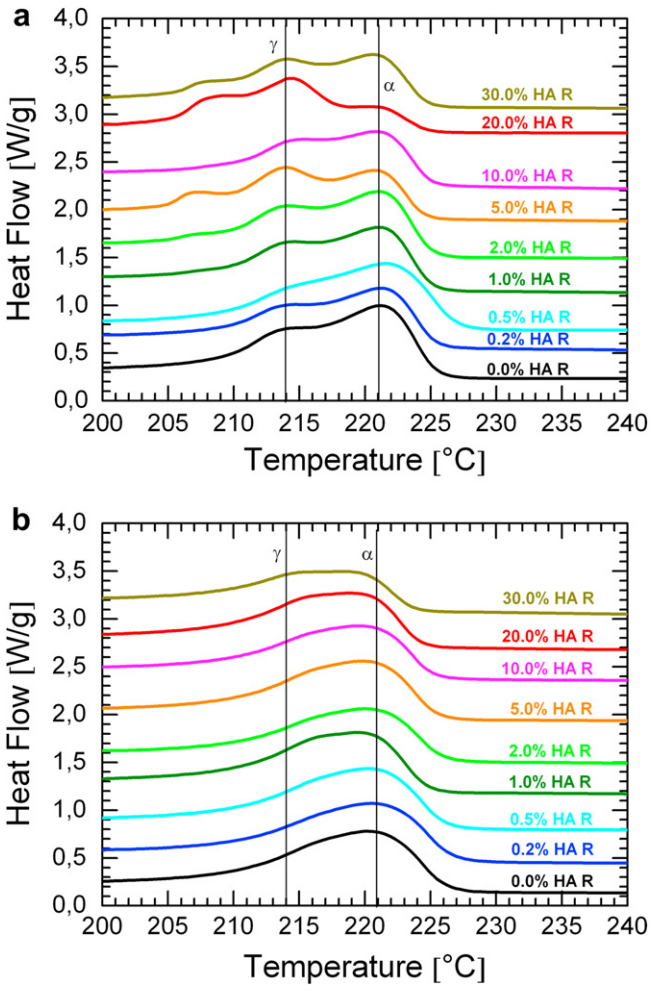

Fig. 4. Results of differential scanning calorimetry measurements of (a) the B27/HA R composites and (b) the B40/HA R composites (second heating cycle). The heating rate was 10 K/min. The data are shifted vertically for clarity.

reveal that both the α-modification and the γ-modification are present in the low molar mass PA 6. Fig. 4(a) also shows that an increase of the concentration of the halloysite nanotubes from 0.1 wt% to 5 wt% leads to a shoulder at lower temperatures in the melting peak for the low molar mass PA 6 B27. This effect is only slightly pronounced for PA 6 B40. The occurrence of a shoulder for the B27/HA G (not shown in the Figure) and the B27/HA R composites reveals that the fraction of the γ-modification is increased by the addition of the silicate nanotubes. In Fig. 4(a) three peaks are visible for the B27/HA R composites with a halloysite concentration above 2 wt% (except for B27/HA R 10). Two of these peaks correspond to the α- and γ-modifications, respectively. The third peak most probably results from recrystallization phenomena during heating. Finally, the analysis of the heating and cooling cycles shows that the glass transition, melting and crystallization temperatures were not altered by the presence of the halloysite fillers, see Table 2.

The X-ray diffraction measurements also underline that both the α- and the γ-modification are present in PA 6 B27 E and the B27/HA G nanocomposites (Fig. 5). The different reflexes are associated with different crystal structures as indicated in Fig. 5. The peak of the γ-modification is located at 21.3°, and the maxima of the α-modifications at 20.0° and 23.7° [12]. With increasing concentration of halloysite the peaks of the α_{002}-, the α_{200}- and the γ_{100}-modification can be clearly distinguished.

Table 2
Composition and thermal properties of the PA 6/halloysite nanocomposites of this study. (a) B27/HA G composites, (b) B27/HA R composites, and (c) B40/HA R composites.

Material	Conc. PA 6 (wt%)	Conc. HA (wt%)	T_g (°C)	T_m (°C)	T_{cryst} (°C)	Crystallinity (%)
(a)						
PA 6 B27	100.0	0.0	54	221	188	26.1
B27/HA G 90/10	90.0	10.0	53	220	189	22.3
B27/HA G 80/20	80.0	20.0	52	220	189	21.5
B27/HA G 70/30	70.0	30.0	53	220	189	21.3
(b)						
PA 6 B27 E	100.0	0.0	54	221	188	22.2
B27 HA R 02	99.8	0.2	53	221	188	22.4
B27 HA R 05	99.5	0.5	53	221	188	23.3
B27 HA R 1	99.0	1.0	52	221	189	23.3
B27 HA R 2	98.0	2.0	53	221	189	22.5
B27 HA R 5	95.0	5.0	53	221	188	21.8
B27 HA R 10	90.0	10.0	55	221	189	24.1
B27 HA R 20	80.0	20.0	53	221	189	20.3
B27 HA R 30	70.0	30.0	53	221	189	26.6
(c)						
PA 6 B40	100.0	0.0	53	220	191	21.5
B40 HA R 02	99.8	0.2	53	220	191	20.3
B40 HA R 05	99.5	0.5	53	220	191	20.9
B40 HA R 1	99.0	1.0	54	220	191	20.5
B40 HA R 2	98.0	2.0	54	220	191	20.6
B40 HA R 5	95.0	5.0	53	220	190	22.0
B40 HA R 10	90.0	10.0	54	220	190	21.8
B40 HA R 20	80.0	20.0	53	219	190	21.2
B40 HA R 30	70.0	30.0	52	219	189	23.3

The results of the dynamic-mechanical experiments are plotted in Fig. 6. Fig. 6(a) and (b) shows the storage modulus G' and the loss modulus G'' as a function of temperature in the range of −120–215 °C for the B27/HA G composites. The storage modulus G' of neat PA 6 continuously decreases with temperature. The two maxima of the loss modulus G'' are associated with the β- and the α-transition (glass transition). The temperatures of the α-peaks of G'' increase from 55.8 °C to 64.9 °C with increasing filler content. The three B27/HA G composites show a shift of the peak around 7–9 °C. This shift is caused by the halloysite nanotubes which increase the dissipation (i.e. the loss modulus G'') above T_g of polyamide 6. Above T_g the amorphous phase is mobile and the presence of halloysite nanotubes increases the energy dissipation during each torsion cycle. This effect shifts the maximum of G'' towards larger temperatures. However, the T_g of the matrix is not

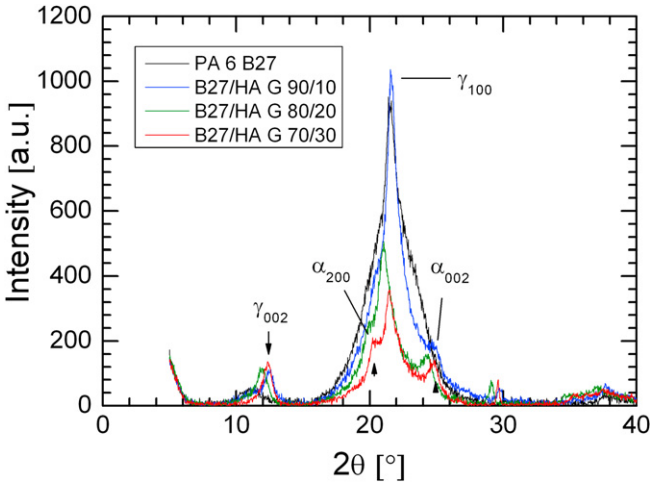

Fig. 5. Results of wide angle X-ray diffraction measurements using extruded pellets of the B27/HA G composites. The scattering angle is denoted by 2θ.

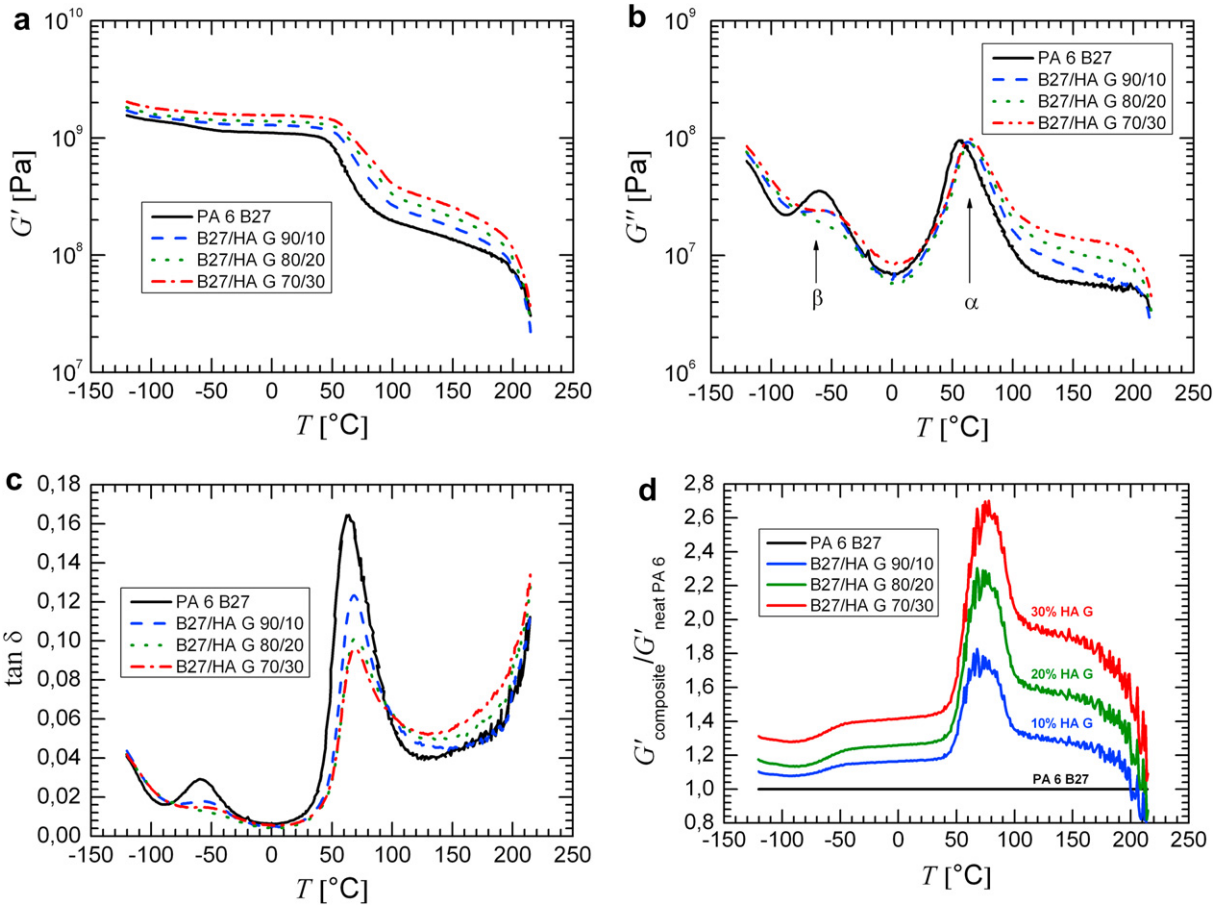

Fig. 6. Complex modulus $G^* = G' + iG''$ measured by dynamic-mechanical experiments at a constant frequency of $f = 1$ Hz, an amplitude of 0.15% and a heating rate of 3 K/min in the torsion mode. (a) Storage modulus G', (b) loss modulus G'', (c) loss tangent $\tan\delta = G''/G'$ and (d) reinforcement factor $G'_{\text{composite}}/G'_{\text{neat PA 6}}$ as a function of temperature.

altered by the halloysite nanotubes as indicated by the DSC data. In Fig. 6(d), the reinforcement factor

$$r = G'_{\text{composite}}/G'_{\text{neat PA 6}} \quad (1)$$

is plotted as a function of temperature T. The data clearly reveal that the addition of halloysite increases at most the modulus in the temperature interval from 55 °C to 100 °C, i.e. above the glass transition temperature of PA 6 where the modulus of PA 6 strongly decreases with T.

3.3. Mechanical properties

One principal objective of this study is the evaluation of the potential of halloysite nanofillers on the mechanical reinforcement of polyamide 6. Mechanical tests were performed at room temperature, i.e. below T_g of PA 6, and at 80 °C, i.e. above T_g of PA 6. Fig. 7(a) presents representative curves of tensile tests (nominal stress vs. nominal strain) using the B27/HA R composites at room temperature. At small strains, polyamide 6 and the PA 6/halloysite composites behave linearly elastic. At larger the strains, yield processes set in. These yield processes take place for composites with a halloysite concentration below 5 wt%, see Fig. 7(a). The curves of neat PA 6 and the composites reveal that with increasing filler fraction the PA 6/halloysite composites become less ductile and the composites behave brittle at a filler fraction above 10 wt%. The increasing brittleness of the composites with halloysite content was also revealed by the work to fracture measured in the tensile tests. The presence of halloysite nanofillers causes stress concentration at the filler surface. Furthermore, interfacial failure is more pronounced with increasing loading of halloysite.

Young's modulus E as a function of halloysite concentration is plotted in Fig. 7(b). At a filler fraction up to 2 wt% the modulus of elasticity is strongly increased for the composites with the low molar mass PA 6 B27. The increase of the modulus is much more pronounced than for the B40/HA R composites. At larger filler fractions, Young's modulus of all composites increases linearly with halloysite concentration. Using the linear rule of mixture, the elastic modulus of halloysite can be estimated and is given by approximately 10060 MPa.

A similar trend as for Young's modulus holds for the yield stress, see Fig. 7(c). The addition of a low fraction of halloysite significantly increases the yield stress of PA 6. As already noted for Young's modulus, the yield stress increases very strongly in a step-wise manner for the low molar PA 6, whereas for the B40/HA R composites a smoother increase is observed.

The ratio $E_{\text{composite}}/E_{\text{neat PA 6}}$ of Young's modulus $E_{\text{composite}}$ of the composites to the modulus $E_{\text{neat PA 6}}$ of neat polyamide 6 quantifies the reinforcement which is caused by the halloysite nanotubes (Fig. 7(d)). The reinforcement increases with filler concentration and attains a value of approximately 1.9 for the composites with 30 wt% halloysite. Furthermore, the reinforcement factor at low filler fractions is slightly larger for the PA 6 B27/HA R composites than for the B40 HA/R composites.

The results of our mechanical tests (nominal stress–strain diagram) at 80 °C are plotted in Fig. 8. At this elevated temperature

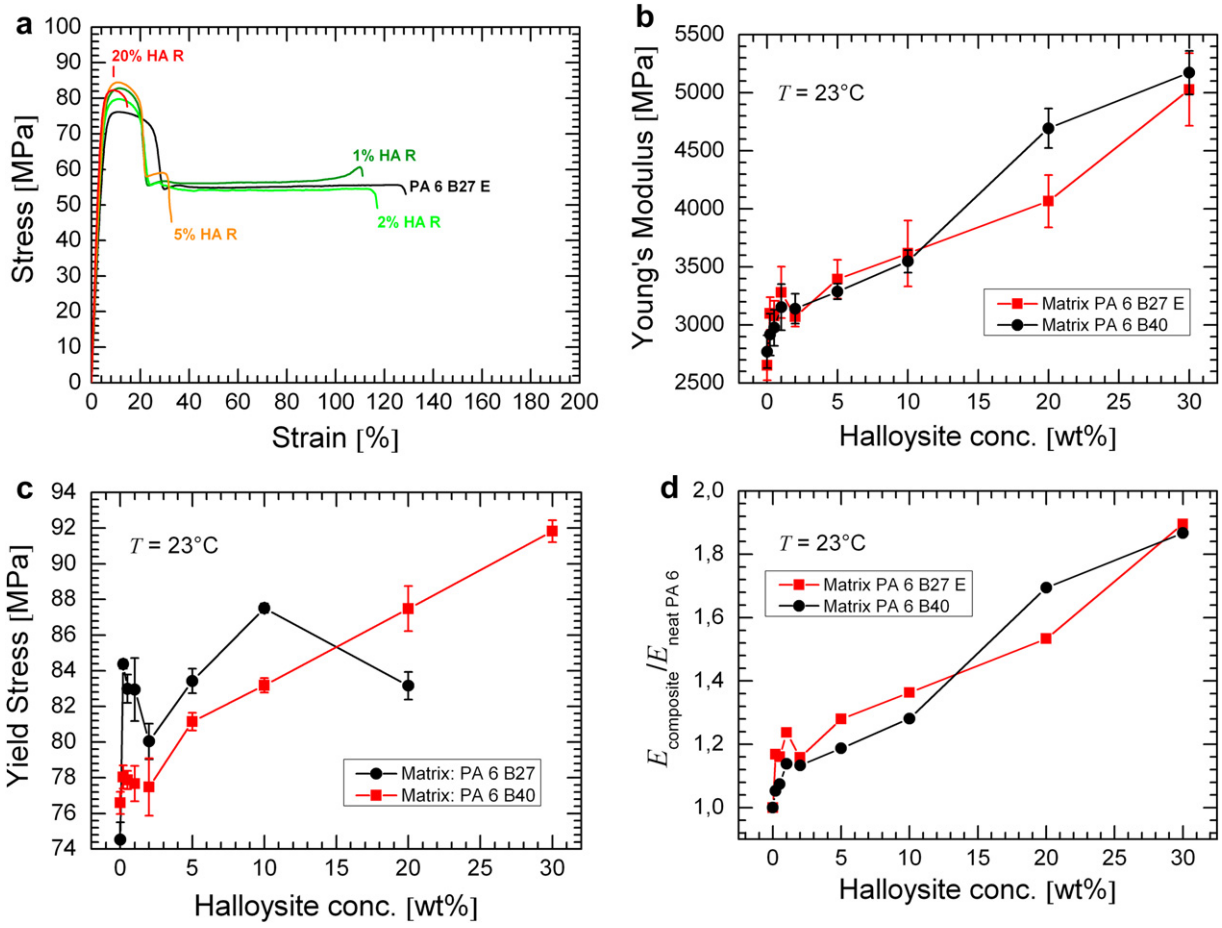

Fig. 7. Mechanical properties of the B27/HA R and B40/HA R series of polyamide 6/halloysite nanocomposites at room temperature. (a) Representative curves of the tensile tests of the B27/HA R composites at room temperature (nominal stress vs. nominal strain). (b) Young's modulus E. (c) Yield stress σ_y. (d) Reinforcement factor $E_{composite}/E_{neat\ PA\ 6}$ for the B27/HA R and the B40/HA R composites.

neat PA 6 and the nanocomposites behave more ductile, since the amorphous phase of PA 6 is not anymore in the glassy state. The modulus of elasticity of the halloysite composites increases with concentration of halloysite. This effect is already pronounced at low filler fractions for the low molar mass polyamide 6 (PA 6 B27 E). Similar to the mechanical properties at room temperature, the B27/HA R composites are associated with a larger increase of modulus at low filler fractions than the B40/HA R composites. Furthermore the elongation at break at this elevated temperature does not decrease in such a drastic way as at room temperature. These results imply that halloysite act as effective reinforcement fillers above the glass transition temperature of PA 6.

3.4. Rheological properties

The analysis of the rheological experiments has to take into account that the molecular weight distribution of PA 6 might change because of degradation and polycondensation in the molten state [36]. Our experiments revealed that the addition of 0.2, 0.5 and 1.0 wt% halloysite does not significantly change the flow properties of PA 6. The effect of the addition of such a low fraction of halloysite is negligible in comparison to the experimental scatter which is enhanced because of the limited thermal stability of PA 6. The zero shear rate viscosity η_0 of PA 6 B27 E is 400 Pa. Because of this low value for polymer melts, the lower limit of rheometer resolution is attained which is indicated by the strongly scattering data at low frequencies. The experimental scatter is less pronounced for the PA 6 with the higher molar mass (PA 6 B40).

The trends which were observed for all three series of PA 6/halloysite composites were similar. Fig. 9 presents the storage modulus G' and the loss modulus G'' of neat PA 6 B40 and the B40/HA R composites. The average relaxation time $\langle\tau\rangle$ of neat PA 6 B40 is in the order of $\langle\tau\rangle = J_e^0\eta_0 \approx G'/(\eta_0\omega^2) \approx 0.1$ s where J_e^0 denotes the equilibrium compliance in the linear viscoelastic regime. Hence the G' and G'' data for $\omega < 1/\langle\tau\rangle \approx 10$ rad/s correspond to the terminal zone with the characteristic power-laws $G' \propto \omega^2$ and $G'' \propto \omega$. Increasing the concentration of the B40/HA R composites leads to a more pronounced deviation from these power-laws. This behaviour is caused by the filler–filler interactions which lead to larger values of G' and G'' in comparison to neat PA 6. At $\omega = 0.1$ rad/s, the complex viscosity of neat PA 6 B40 is given by 3500 Pa s and for the B40 HA R 30 composite by 13800 Pa s. Interestingly, even at the largest filler fraction (30 wt%) no indication of a solid-like behaviour (plateau of G' at low frequencies) can be observed.

Capillary experiments allow one to determine the flow properties at large shear rates. Fig. 10 presents the results of the capillary measurements as well as the complex viscosity η^* as a function of shear rate. Although some discrepancy for the B40/HA R series exists, a violation of the Cox–Merz rule $\eta(\dot\gamma) = |\eta^*(\omega)|$ with $\dot\gamma = \omega$ cannot be stated for neat PA 6 and the halloysite composites. At low shear rates, a Newtonian plateau exists for neat PA 6 and the PA 6/halloysite composites and the viscosity increases with filler loading. Even at the largest filler concentration, only a very weak tendency

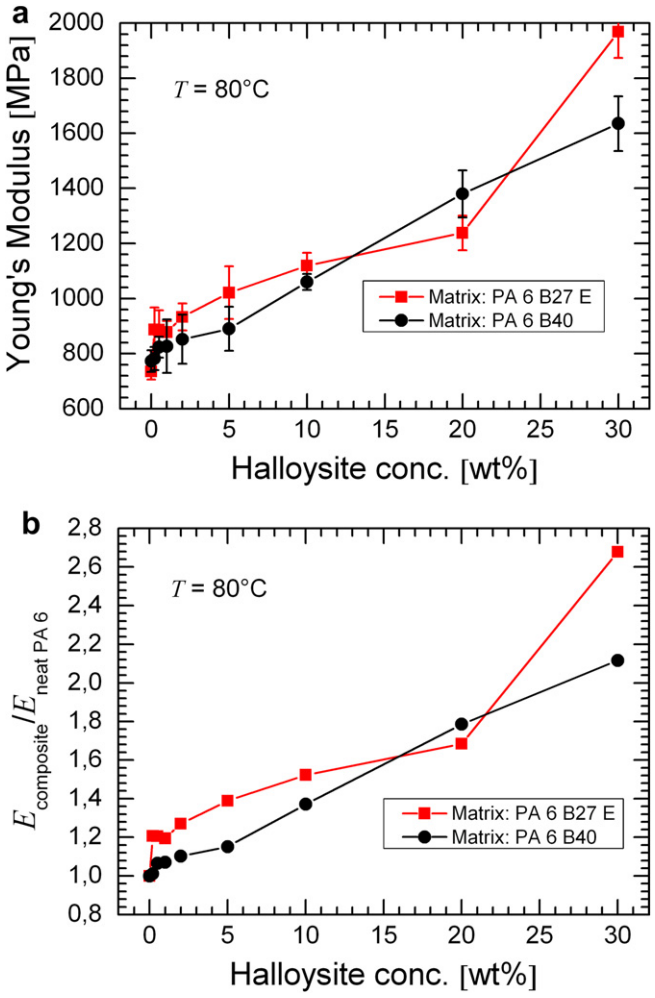

Fig. 8. Results of tensile tests of the B27/HA R and the B40/HA R composites at 80 °C. (a) Young's modulus E. (b) Reinforcement factor $E_{composite}/E_{neat\ PA\ 6}$ at 80 °C.

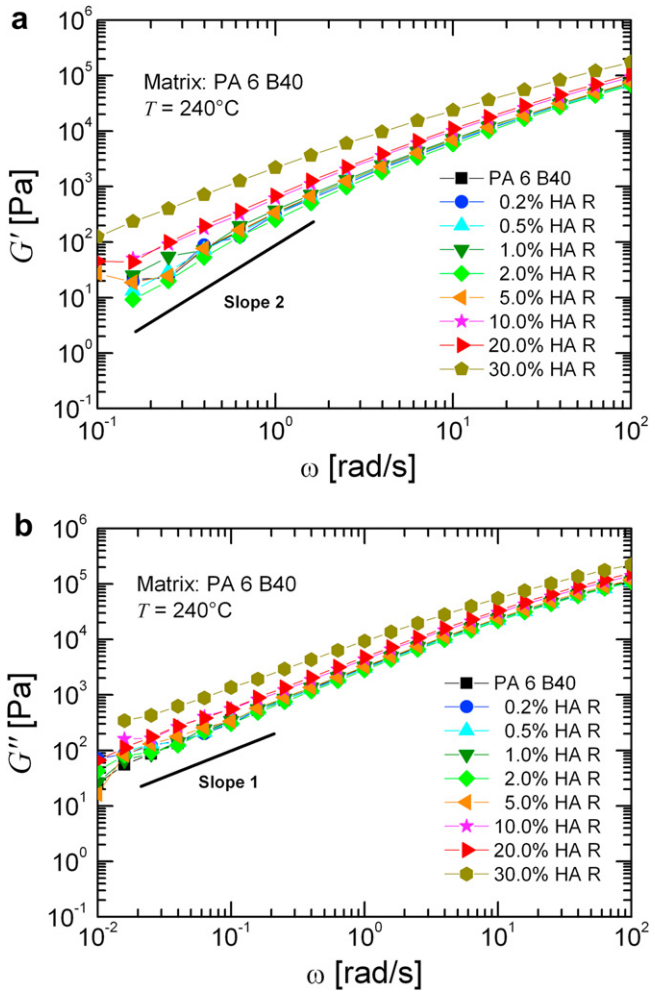

Fig. 9. (a) Storage modulus G' and (b) loss modulus G'' of melts of PA 6 nanocomposites filled with halloysite nanotubes (B40/HA R series). The matrix material was PA 6 B40, and the test temperature was 240 °C.

to a network can be observed. At larger shear rates, however, the increase of viscosity with filler loading is less pronounced, since at large shear rates the filler–filler interactions are much lower than the shear stress in the matrix.

Using the Rheotens apparatus, the melt elongational properties of neat PA 6 and the PA 6/halloysite composites with varying halloysite concentration were probed. In Fig. 11 the results for the B27/HA G composites are shown. Generally, the force which was measured by the Rheotens apparatus was close to the limit of resolution of the Rheotens apparatus. The force increases with the velocity v of the wheels for all materials. Increasing the filler fraction results in a larger force F, an effect which agrees well with the measurement of the shear viscosity. Furthermore, at large filler fractions the drawability of the PA 6/halloysite nanocomposites is smaller than the drawability of neat PA 6 because of percolation of neighboured nanotubes which leads to breakage of the strand.

4. Discussion

The scanning electron micrographs reveal that single halloysite nanotubes can be uniformly dispersed in polyamide 6. However, in the neat halloysite powder clusters are also present. These agglomerates were not broken up during extrusion and decreased the mechanical performance because of stress concentration at large agglomerates. It seems that the cohesion of the nanotubes within a cluster is much larger than the shear stress which is caused by the surrounding PA 6 matrix. Since the processing temperature was close to the melting temperature of the semi-crystalline PA 6, a further reduction of extrusion temperature was impossible. The formation of aggregates can be possibly avoided by an optimum surface modification of halloysite.

The addition of elastic fillers mostly increases the stiffness of the material, whereas the melt viscosity is only moderately influenced. To a first approximation, the tensile modulus results from a rule of mixture and is a function of the moduli of the matrix and filler, concentration and aspect ratio of the filler [37]. On the contrary, the viscosity is only increased by a factor which is in the order of $1 + 2.5\Phi$, where Φ denotes the volume fraction [38]. Hence the increase of melt viscosity is much smaller than the reinforcement in the solid state.

The increase of the elastic moduli is very dominant at low filler contents. This effect is clearly seen for the low molar mass PA 6 B27 E and less pronounced for the high molar mass PA 6 B40. The DSC and WAXD data suggest that the mechanical properties are influenced by the effect of halloysite nanotubes on the crystallization behaviour of PA 6. In a recent work, the crystallization behaviour of several polyamide 6 nanocomposites was studied [39,40]. These studies revealed that clay nanofillers promote the formation of the γ-modification of PA 6. A possible explanation of the reinforcement effect which is evident at low filler fractions is the influence of

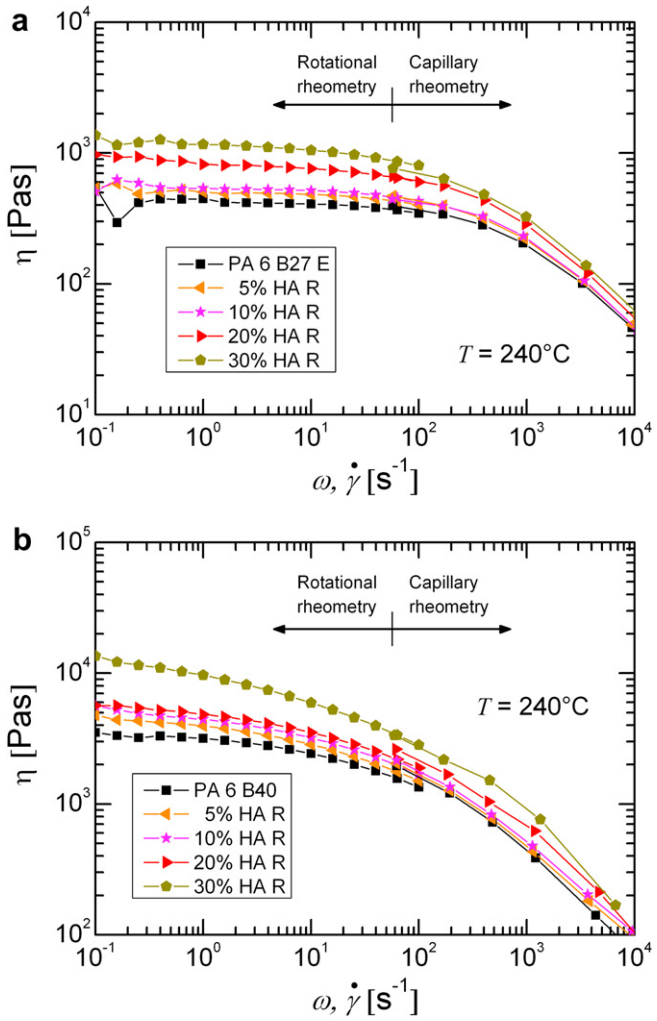

Fig. 10. Complex viscosity $|\eta^*|$ and stationary viscosity η as a function of ω and shear rate $\dot{\gamma}$, respectively, at 240 °C for (a) PA 6 B27 E and the B27/HA R composites and (b) PA 6 B40 and the B40/HA R nanocomposites.

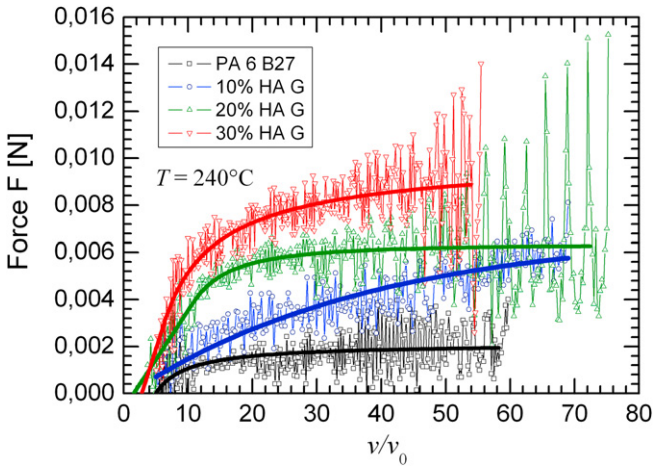

Fig. 11. Measured force F as a function of v/v_0 in Rheotens experiments at 240 °C for neat polyamide 6 and the B27/HA G composites. The weight concentration of halloysite is indicated.

halloysite on the crystallization behaviour. Halloysite nanotubes act as nucleating agent and cause an effective arrangement of the crystalline phase. At larger filler fractions, however, the mixing effect of the elastic properties of PA 6 and halloysite dominates.

The results for the polyamide 6/halloysite nanocomposites can be compared with a related study on PA 6/organoclay nanocomposites [11,41]. In the study of Fornes et al. three different PA 6 were used with different molecular weights [11]. The mechanical properties of the nanocomposites showed the best performance for the PA 6 composites with the largest molecular weight. This effect was explained by the highest degree of exfoliation in the composites with the high molecular weight PA 6. In contrast to layered silicate, halloysite nanotubes cannot be exfoliated. Hence the effective surface area is much lower for the halloysite nanocomposites than for the organoclay composites. In this work, the effect of the addition of halloysite is mostly pronounced for the composites with the lower molecular weight. In our case, halloysite influences the crystallization behaviour, in particular for the low molar mass PA 6 with the shorter polymer chains. Hence, the reinforcement effect is mostly pronounced for the PA 6/halloysite composites with the low molar mass PA 6, in particular above T_g of PA 6.

5. Conclusions

In this work, the influence of the molar mass of polyamide 6 on the thermal, mechanical and rheological properties of PA 6/halloysite nanocomposites was studied. The addition of halloysite clearly increases the modulus and the yield stress of polyamide 6, an effect which is very much pronounced at low filler fractions for the low molar mass PA 6. At large filler fractions, the modulus of elasticity and the storage modulus linearly increase with concentration of halloysite. The addition of 30 wt% halloysite leads to an increase of Young's modulus in the order of 90%. The reinforcement effect of halloysite nanotubes is very dominant above the glass transition temperature of PA 6. Furthermore, halloysite nanotubes influence the crystallization behaviour of PA 6 and favour the formation of the γ-modification for the low molar mass PA 6. This result suggests that the reinforcement effect at low filler fractions is possibly caused by the formation of an effective arrangement of the crystalline phase in the presence of halloysite. The flow properties of polyamide 6 are only moderately altered by the addition of halloysite nanotubes. Even at a filler concentration of 30 wt% no indication of a filler network was observed. Hence PA 6/halloysite composites can be still processed under similar conditions as neat polyamide 6. In summary, halloysite nanotubes clearly improve the elastic properties of PA 6 in the solid state without loosing the very good flow properties of PA 6. Consequently, halloysite is a very interesting alternative to kaolin and wollastonite. By adequately selecting halloysite nanotubes with a high aspect ratio, composites with a high potential for applications can be obtained.

Acknowledgements

The authors are very grateful to the Deutsche Forschungsgemeinschaft for financial support of this work (DFG project no. AL 474/13-1) and to Imerys Tableware Ltd., in particular to Dr. David Gittins and Dr. Chris Paynter, for supplying the mineral halloysite. They are also thankful to Dr. Helmut Steininger and Dr. Martin Weber (BASF SE, Ludwigshafen, Germany) for very valuable discussions. WAXD measurements by Dr. Wolfgang Milius and the experimental support of Mr. Alexander Brückner, Mr. Vitaliy Demchuk, Mr. Frank Fischer, Mr. Christian Götz, Mr. Christian Hugel, Mrs. Romica Kiesewetter, Mrs. Ute Kuhn, Mrs. Carmen

Kunert, Mrs. Anne Lang, Mr. Andreas Mainz, Mrs. Jacqueline Uhm and Mr. Marko Weniger are gratefully acknowledged.

References

[1] Mittal V. J Thermoplast Compos Mater 2007;20:575–99.
[2] Mittal V. Materials 2009;2:992–1057.
[3] Cadek M, Coleman JN, Barron V, Hedicke K, Blau WJ. Appl Phys Lett 2002;81 (27):5123–5 [Erratum. Appl Phys Lett 2003;83(13):2718].
[4] Wang C, Guo ZX, Fu S, Wu W, Zhu D. Prog Polym Sci 2004;29(11):1079–141.
[5] Zeng QH, Yu AB, Lu GQ. Prog Polym Sci 2008;33:191–269.
[6] Chen B, Evans JRG, Greenwell HC, Boulet P, Coveney PV, Bowden AA, et al. Chem Soc Rev 2008;37:568–94.
[7] Bokobza L. Polymer 2007;48(17):4907–20.
[8] Utracki LA, Sepehr M, Boccaleri E. Polym Adv Technol 2007;18:1–87.
[9] Coleman JN, Khan U, Blau WJ, Gun'ko YK. Carbon 2006;44:1624–52.
[10] Heinrich G, Klüppel M, Vilgis TA. Curr Opin Solid State Mater Sci 2002;6: 195–203.
[11] Fornes TD, Yoon PJ, Keskkula H, Paul DR. Polymer 2001;42:9929–40 [Erratum. Polymer 2002;43:2121–2122].
[12] Fornes TD, Paul DR. Polymer 2003;44:3945–61.
[13] Kim GM, Lee DH, Hoffmann B, Kressler J, Stöppelmann G. Polymer 2001;42: 1095–100.
[14] Handge UA, Pötschke P. Rheol Acta 2007;46:889–98.
[15] Hedicke-Höchstötter K, Demchuk V, Langenfelder D, Altstädt V. J Plast Technol 2007;3(2):1–22.
[16] Singh B. Clays Clay Miner 1996;44(2):191–6.
[17] Unal H, Mimaroglu A, Alkan M. Polym Int 2004;53:56–60.
[18] Maiti SN, Lopez BH. J Appl Polym Sci 1992;44:353–60.
[19] Ariffin A, Mansor AS, Jikan SS, Ishak ZAM. J Appl Polym Sci 2008;108: 3901–16.
[20] Ye Y, Chen H, Wu J, Ye L. Polymer 2007;48:6426–33.
[21] Deng S, Zhang J, Ye L, Wu J. Polymer 2008;49:5119–27.
[22] Liu M, Guo B, Du M, Cai X, Jia D. Nanotechnology 2007;18:455703.
[23] Liu M, Guo B, Zou Q, Du M, Jia D. Nanotechnology 2008;19:205709.
[24] Liu M, Guo B, Du M, Cheng F, Jia D. Polymer 2009;50:3022–30.
[25] Du M, Guo B, Cai X, Jia Z, Liu M, Jia D. e-Polymers; 2008:130.
[26] Guo B, Zou Q, Lei Y, Du M, Liu M, Jia D. Thermochim Acta 2009;484:48–56.
[27] Ning NY, Yin QJ, Luo F, Zhang Q, Du R, Fu Q. Polymer 2007;48:7374–84.
[28] Du M, Guo B, Jia D. Eur Polym J 2006;42:1362–9.
[29] Marney DCO, Russell LJ, Wu DY, Nguyen T, Cramm D, Rigopoulos N, et al. Polym Degrad Stab 2008;93:1971–8.
[30] Du M, Guo B, Liu M, Jia D. Polym J 2006;38:1198–204.
[31] Guo B, Zou Q, Lei Y, Jia D. Polym J 2009;41:835–42.
[32] Hedicke-Höchstötter K, Altstädt V. J Plast Technol 2009;5(1):71–86.
[33] Hedicke-Höchstötter K, Lim GT, Altstädt V. Compos Sci Technol 2009;69: 330–4.
[34] Hiramatsu N, Hirakawa S. Polym J 1982;14(3):165–71.
[35] Dasgupta S, Hammond WB, Goddard III WA. J Am Chem Soc 1996;118: 12291–301.
[36] Laun HM. Rheol Acta 1979;18:478–91.
[37] Halpin JC, Kardos JL. Polym Eng Sci 1976;16:344–52.
[38] Einstein A. Ann Phys 1906;19:289–306 [Erratum. Annal Phys 1911;34: 591–592].
[39] Hedicke K, Wittich H, Mehler C, Gruber F, Altstädt V. Compos Sci Technol 2006;66:571–5.
[40] Bureau MN, Denault J, Cole KC, Enright GD. Polym Eng Sci 2002;42(9): 1897–906.
[41] Cho JW, Paul DR. Polymer 2001;42:1083–94.